

Short-term forecasting of Italian residential gas demand

Andrea Marziali^{1,2}, Emanuele Fabbiani², and Giuseppe De Nicolao²

¹Modelling and pricing, A2A

²Department of Electrical, Computer and Biomedical Engineering,
University of Pavia

4th May 2022

Abstract

Natural gas is one of the most important energy sources in Italy: it fuels thermoelectric power plants, industrial facilities and domestic heating. Forecasting gas demand is a critical process for each energy provider, as it enables pipe reservation and stock planning. In this paper, we address the problem of short-term forecasting of residential gas demand by comparing several statistical learning models, including Ridge regression, Gaussian processes, and neural networks. We also present the preliminary steps of preprocessing and feature engineering. To the best of our knowledge, no benchmark is available for the task we performed, thus we derive a theoretical performance limit, based on the inaccuracy of meteorological forecasts. Our best model, a deep neural network, achieves an RMSE which is double with respect to the performance limit.

Keywords— natural gas; time series forecasting; statistical learning; Gaussian processes; neural networks

1 Introduction

In Italy, natural gas is the most common fuel for both power plants and domestic heating. Moreover, several industrial facilities burn gas for both heating and powering productive processes. According to SNAM Rete Gas [1], the Italian Transmission System Operator (TSO), in 2017 about 70.59 billions of cubic meters of natural gas were consumed, with an increase of 5.6% over the previous year. Overall, the increase in demand between 2015 and 2017 was 11%. Out of the total gas demand in 2017, 35.9% was due to thermoelectric power plants, 22.4% to industrial facilities and 41.7% to residential users.

Forecasting natural gas demand is a key task for energy companies for several reasons. It provides relevant information to effectively reserve pipe capacity and plan stocks. Furthermore, energy regulations impose the balance of the network by charging providers with a fee proportional to their unbalanced quantity. Finally, demand is a critical input to forecast gas price, which is in turn key for several business decisions.

The literature about gas demand forecasting is quite large: comprehensive reviews are [15] and [16]. According to Sebalj et al, papers can be classified by four aspects. The *prediction horizon* can range from hourly to yearly, the *reference area* from single nodes of the network to a whole country; adopted *models* include time series, mathematical and statistical approaches, neural networks (ANN) and others; input *features* can be demand history, temperature, calendar and other minor ones. Our study focuses on day-ahead forecasting of Italian Residential Gas Demand (RGD): we tune and compare five statistical learning models with an input dataset made of 22 features derived from the calendar, past gas demand and forecasted temperature.

Many previous studies focus on country- or regional-level daily forecasting. Mathematical and statistical models based on parametric non-linear functions are used in [4] to explain the factors which affect the demand. A different multi-factor approach is developed in [13] and a model based on the physical relation between gas demand and temperature is presented in [6]. An adaptive network-based fuzzy inference system (ANFIS) is described in [3], where the authors show the better performances of their model with respect to ANN and conventional time series methods. A statistical learning model, based on support vector machine (SVM), is developed in [21] for UK demand, and compared with ANN and an autoregressive moving average (ARMA). A hybrid model, exploiting many different techniques such as wavelet transform, genetic algorithm, ANFIS and ANN is used in [12].

Neural networks are popular and effective models to predict gas demand: they are applied in [19, 5, 18, 17, 20] to perform hourly and daily forecasts on cities and regions.

To the best of our knowledge, no study about the Italian RGD has been published yet. This paper thus provides with insights about the features of the series and its relations with exogenous variables and with baselines for future studies. Because of the lack of benchmarks, to assess the goodness of our models we developed a performance limit based on the inaccuracy of weather forecasts, a critical input for any Italian RGD model.

The paper is organized as follows. In Section 2, we define the task we want to address and present the available data. In Section 3, we provide a statistical characterization of target and input variables and we present preprocessing and feature engineering. Section 4 describes models, training process and hyperparameter tuning, providing some insight about the implementation. In Section 5 we derive the performance limit, which is used as the ultimate benchmark in Section 6, where the results are presented and discussed. Finally, Section 7 is devoted to concluding remarks and possible future developments.

2 Problem Statement

The task addressed in this paper is the one-day-ahead forecasting of daily Italian RGD. Residential demand represents the main part of the overall Italian gas consumption, accounting for household usage for cooking, water heating and, most importantly, environment heating.

Available data cover 11 years, from 2007 to 2017 and are made of 3 fields: date (t), forecasted average temperature (T) and residential gas demand (RGD). Forecasted temperature is provided by Meteologica, a well-known service, and is relative to the Northern regions of Italy. In the preliminary analysis, we also took into consideration a weighted average of the temperatures in different zones of Italy, but we noticed a weaker correlation with RDG. This is explained by the role of domestic heating in Northern Italy whose winters are obviously colder.

The profile of RGD from 2007 to 2017 is displayed in Fig. 1.

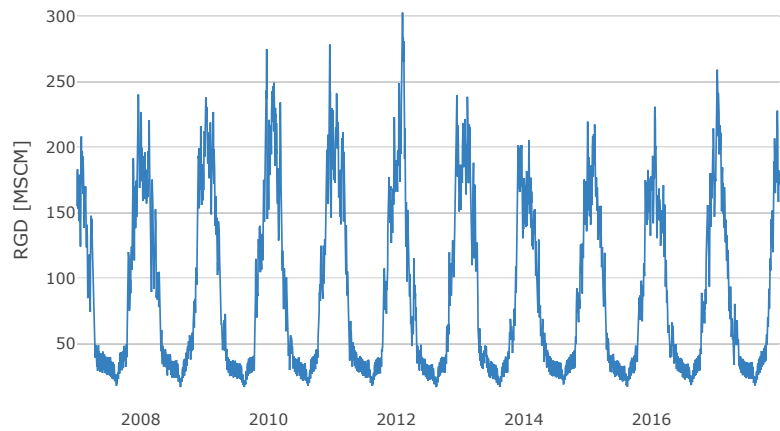


Figure 1: Italian Residential Gas Demand (RGD): years 2007-2017

3 Exploratory analysis and feature selection

3.1 Residential Gas Demand

RGD magnitude greatly oscillates with the season: during the cold months, from October to March, it represents about 56% of the overall Italian demand, while it drops to about 28% during the warm months, from April to September. In fact, when the temperature climbs above 17-18 Celsius degrees, domestic heating is typically switched off. Thus, during the cold period lower temperatures cause a larger RGD, while, during summer, weather influence is negligible, while a seasonal pattern becomes evident, with lower RGD during weekends compared with working days. Due to the

lack of dependence on weather conditions, the profile of summer RGD is remarkably repeatable from year to year. All these features are clearly visible in Fig. 2, which displays eleven years of Italian RGD, overlapped with a proper shift to align weekdays.

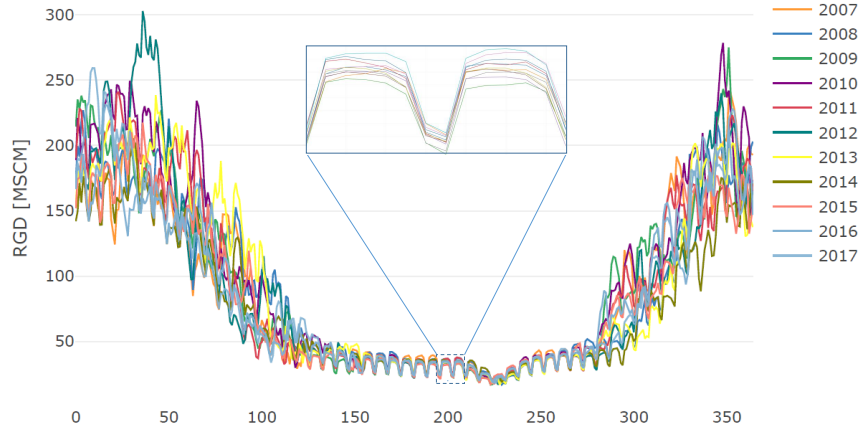


Figure 2: Italian Residential Gas Demand (RGD): years 2007-2017. The time series are shifted to align weekdays: weekly periodicity is particularly visible in summer. The yearly seasonal variation is mostly explained by heating requirements. In the inset, two weeks of July's demand data are zoomed

As expected, the autocorrelation function estimated on the whole 2007-2017 dataset exhibits a clear yearly seasonality and a much smaller weekly periodicity, see Fig. 3.

Most of the spectral density, see Fig. Fig. 4, is concentrated at period 365.25 days. A smaller yet relevant spike can be found at a period of 7 days, accounting for the weekly periodicity. In both cases, smaller peaks at lower periods are ascribable to harmonics.

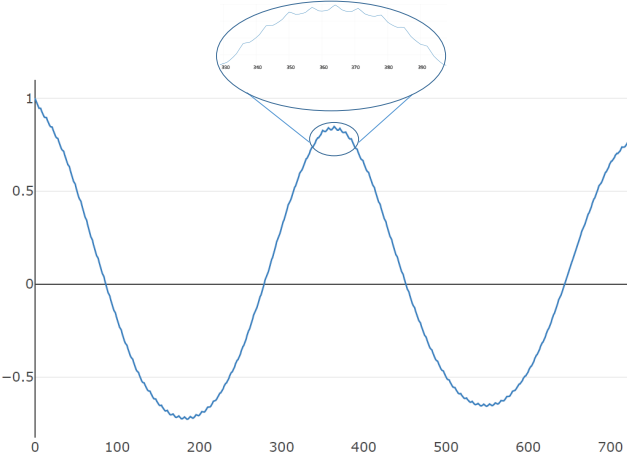


Figure 3: RGD autocorrelation function estimated on 2007-2017 data. The 365-day yearly periodicity is evident. In the inset, weekly waves witness the presence of a 7-day periodicity of much smaller amplitude

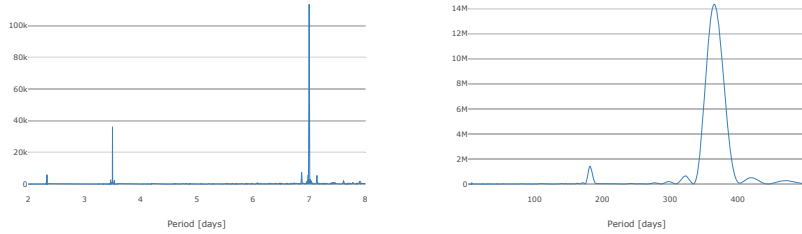


Figure 4: RGD periodogram. Left panel: periods from 0 to 8 days; right panel: periods from 0 to 500 days. The yearly periodicity is highlighted by peaks at 356.25 days, while the weekly one by the smaller spike at a period of 7 days. Other notable values are caused by harmonics

The autocorrelation of lag 1 can be assessed through the scatter plot in Fig. 5a, where RGD at time t is plotted against RGD at time $t - 1$. The correlation coefficient computed on the entire dataset is 0.988, and it increases to 0.995 if Saturdays and Mondays are discarded. This is an evidence of a different behavior between working days and weekends, visually confirmed in the plot, where Monday's RGD (orange dots) stays in the upper part of the cloud whereas Saturday's RGD (green dots) lie in the lower part.

As for the lag-7 autocorrelation, in Fig. 5b the scatter plot of RGD at times t and $t - 7$ is displayed. The scatter plot in Fig. 5b is narrower when the demand is low, that is during warm months, while it gets wider in winter when the demand is high. This is due to the variability of weather from one week to the next one.

In order to characterize the yearly seasonality, it is convenient to introduce the notion of similar day. The following definitions hold:

- $\text{year}(t)$ is the year to which day t belongs;
- $\text{weekday}(t)$ is the weekday of day t , e.g. Monday, Tuesday, etc;
- $\text{yearday}(t)$ is the day number within $\text{year}(t)$ starting from January 1, whose *yearday* is equal to 1.

Definition 1 (Similar Day). *If t is not a holiday, its similar day $\tau^* = \text{sim}(t)$ is*

$$\tau^* = \arg \min_{\tau} |\text{yearday}(\tau) - \text{yearday}(t)|$$

subject to

- $\text{year}(\tau) = \text{year}(t) - 1$;
- $\text{weekday}(\tau) = \text{weekday}(t)$;
- τ is not a holiday.

If t is a holiday, its similar day $\tau^ = \text{sim}(t)$ is the same holiday in the previous year.*

According to the Italian calendar, holidays are: 1 January, 6 January, 25 April, 1 May, 2 June, 15 August, 1 November, 8, 25 and 26 December, Easter and Easter Monday.

The relationship between RGD and RGD in the similar day is shown in Fig. 5c: again, the correlation is higher when the demand is lower, due to the smaller influence of temperature.

It can also be of some interest to take into account the similar day of $t - 1$. The scatter plot in Fig. 5d shows that the difference $RGD(t - 1) - RGD(\text{sim}(t - 1))$ is a very good proxy to the difference $RGD(t) - RGD(\text{sim}(t))$.

Due to these considerations, we use $RGD(t - 1)$, $RGD(t - 7)$, $RGD(\text{sim}(t))$, and $RGD(\text{sim}(t - 1))$ as inputs to forecast RGD at time t .

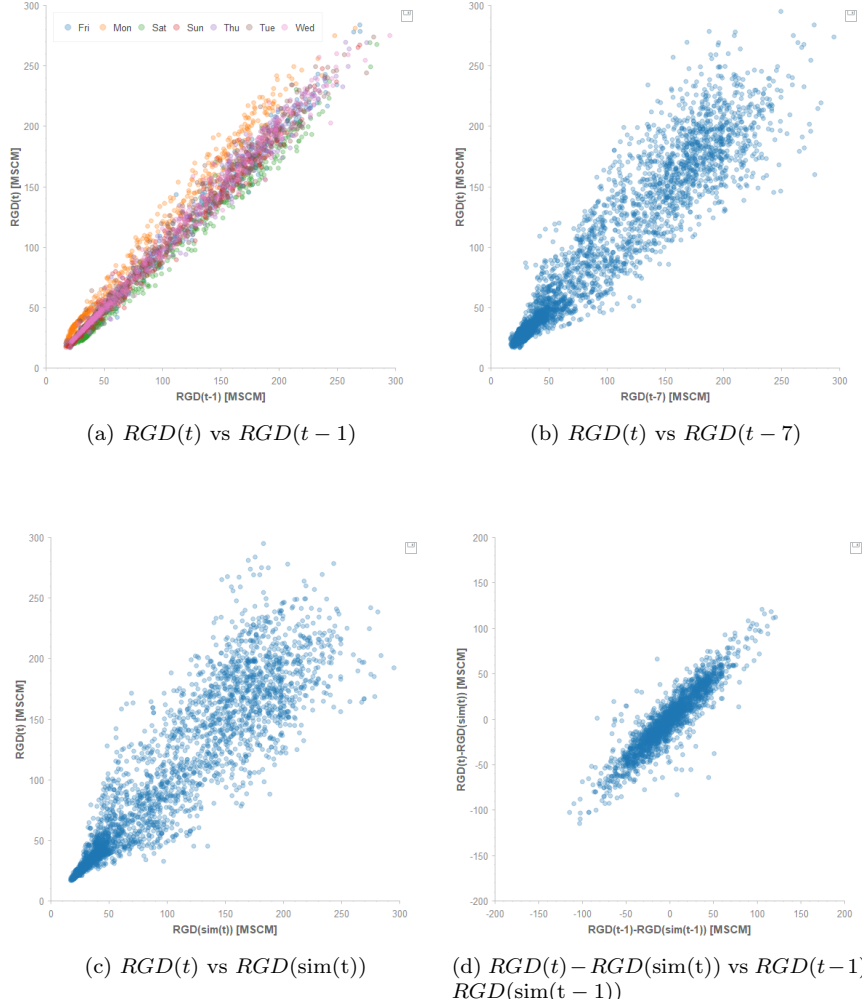


Figure 5: Scatter plots between RGD and potential features to be used for its prediction

3.2 Temperature

The RGD time series shows a strong relationship with temperature, especially when, during the winter season, temperature falls below $18^\circ C$ and household heating becomes relevant. As shown in the left panel of Fig. 6, the relationship is piecewise linear: a line with negative slope below $18^\circ C$, followed by an approximately constant line above $18^\circ C$. In order to transform the piecewise linear dependence into a linear one, it is useful to make reference to the so-called Heating Day Degrees (HDD):

Definition 2 (Heating Day Degrees (HDD)).

$$HDD(T) = \max(18^\circ - T, 0) \quad (1)$$

In the right panel of Fig. 6, the scatter plot of RGD vs HDD highlights an approximately linear relationship, with a positive correlation of 0.97. The correlation of HDD

with RGD is even more evident when we look at the time series of RGD and HDD during 2017, see Fig. 7.

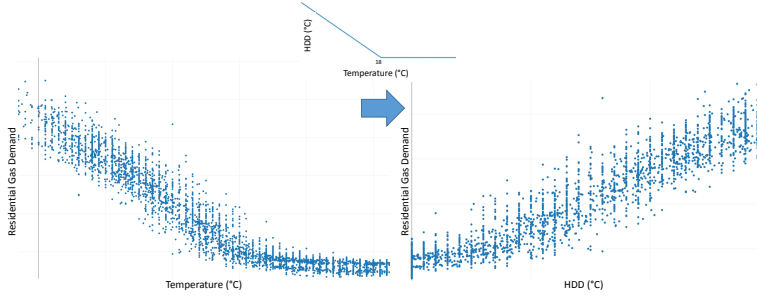


Figure 6: Left panel: scatter plot of daily RGD vs average daily temperature. Right panel: scatter plot of daily RGD vs HDD. Inset: HDD as a function of the temperature

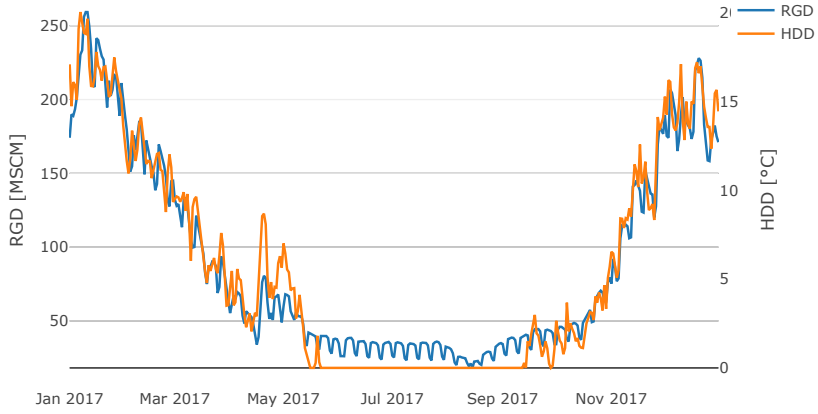


Figure 7: Time series of RGD and HDD in 2017. The instantaneous correlation between the two series is apparent

As shown in Fig. 6, HDD are more correlated to gas demand than plain temperatures. Thus, we consider $\text{HDD}(\hat{T}(t))$ as a feature, where $\hat{T}(t)$ denotes the one-day-ahead forecast of $T(t)$. As additional features also $\text{HDD}(\hat{T}(t-1))$, $\text{HDD}(\hat{T}(t-2))$

Feature	Reference time	Type
RGD	t-1	continuous
RGD	t-7	continuous
RGD	sim(t)	continuous
RGD	sim(t - 1)	continuous
Forecasted temperature	t	continuous
Forecasted temperature	t-1	continuous
Forecasted temperature	t-7	continuous
Forecasted temperature	sim(t)	continuous
Forecasted HDD	t	continuous
Forecasted HDD	t-1	continuous
Forecasted HDD	t-7	continuous
Forecasted HDD	sim(t)	continuous
Weekday	t	categorical
Holiday	t	dummy
Day after holiday	t	dummy
Bridge holiday	t	dummy

Table 1: Features

$\hat{T}(t)$), $\text{HDD}(\hat{T}(\text{sim}(t)))$ are included. For completeness, also $\hat{T}(t)$, $\hat{T}(t - 1)$, $\hat{T}(t - 7)$ and $\hat{T}(\text{sim}(t))$ are included.

3.3 Calendar features

As shown in the previous paragraphs, weekdays and holidays have a great influence on RGD. To capture this phenomena, the following categorical calendar features are taken into account.

Weekday. In view of the weekly periodicity, the seven days of the week are taken as explanatory features. By resorting to the one-hot encoding method they are transformed in n dichotomic time series with $n = 7$.

Holiday. A binary feature which takes value 1 in correspondence of holidays.

Day after holiday. A binary feature which takes value 1 the first working day after a holiday. A working day is a day different from Saturday or Sunday that is not a holiday.

Bridge holiday. A binary feature which takes value 1 on isolated working days, that is working days where both the day before and the day after are either Saturdays, Sundays or holidays.

All the features are summarized in Table 1

4 Prediction models

The classical methods used for time series forecasting are linear Box-Jenkins models such as *SARIMA*, where the forecast is based only on past values of the time series, and

SARIMAX, that accounts also for exogenous variables. A major drawback of classical linear models is given by discontinuities due to holidays and the possible presence of other nonlinear phenomena. In order to overcome these difficulties, herein RGD forecasting is formulated as a machine learning problem.

Based on the availability of n data pairs (\mathbf{x}_i, y_i) , $i = 1, \dots, n$, known as the training data, a prediction rule $f(\cdot)$ is designed with the objective of using $f(\mathbf{x}_*)$ as prediction of y_* , where (\mathbf{x}_*, y_*) is any novel input-output pair. In this context, $\mathbf{x}_i \in \mathbb{R}^p$, $p < n$, is a vector whose entries are given by the p features associated with the target y_i .

Herein, the p features are the 22 covariates (continuous and categorical) discussed in the previous section and shown in Table 1. In the following, with reference to the training data, $\mathbf{y} = y_i \in \mathbb{R}^n$ will denote the vector of the targets and $\mathbf{X} = \{\mathbf{x}_{ij}\} \in \mathbb{R}^{n \times p}$ will denote the matrix of the training input data, where x_{ij} is the j -th feature of the i -th training pair (\mathbf{x}_i, y_i) .

Below, five approaches are presented:

- ridge regression;
- torus model [8];
- Gaussian Process (GP);
- k-nearest neighbour (KNN);
- artificial neural network (ANN).

4.1 Ridge regression

Ridge regression [9] is a technique to identify a linear model in the form:

$$\hat{f}(\mathbf{x}) = \sum_{j=1}^p x_{ij} \beta_j = \mathbf{X}\boldsymbol{\beta}, \quad \boldsymbol{\beta} \in \mathbb{R}^p$$

To prevent overfitting, besides the standard squared sum of the residuals, the loss function includes the squared norm of the parameter vector $\boldsymbol{\beta}$:

$$\boldsymbol{\beta}^{\text{ridge}} := \arg \min_{\boldsymbol{\beta}} \|\mathbf{y} - \mathbf{X}\boldsymbol{\beta}\|^2 + \lambda \|\boldsymbol{\beta}\|^2 \quad (2)$$

where λ is the so-called regularization parameter that plays the role of *hyperparameter*, which controls the flexibility of the learning algorithm. Assuming that \mathbf{X} is full rank, the solution of (2) is

$$\boldsymbol{\beta}^{\text{ridge}} = (\mathbf{X}^T \mathbf{X} + \lambda \mathbf{I})^{-1} \mathbf{X}^T \mathbf{y} \quad (3)$$

that highlights the shrinking effect with respect to the standard least squares estimator $\boldsymbol{\beta}^{LS} = (\mathbf{X}^T \mathbf{X})^{-1} \mathbf{X}^T \mathbf{y}$.

Since the parameters are obtained in closed form (3), the ridge regression model is completely specified by the choice of λ , that can be calibrated following different approaches [9].

4.2 Gaussian processes

Let $\bar{\mathbf{y}} = [y^* \ \mathbf{y}^T]^T$, $\bar{\mathbf{x}} = [\mathbf{x}^{*T} \ \mathbf{x}_1^T \ \dots \ \mathbf{x}_n^T]^T$ and assume that, conditional on $\bar{\mathbf{x}}$, the vector $\bar{\mathbf{y}}$ is normally distributed as follows

$$\begin{aligned}\bar{\mathbf{y}}|\bar{\mathbf{x}} &\sim \mathcal{N}(\mathbf{0}, \Sigma(\bar{\mathbf{x}}) + \sigma^2 \mathbf{I}_n) \\ [\Sigma(\bar{\mathbf{x}})]_{ij} &= \kappa(\bar{x}_i, \bar{x}_j)\end{aligned}$$

where the *kernel* $\kappa(\cdot, \cdot)$ is a suitable function whose choice reflects the available prior knowledge on the characteristics of the prediction rule. It is worth noting that the previous hypothesis is equivalent to assuming that

$$y_i = f(\mathbf{x}_i) + \epsilon_i, \quad i = 1, \dots, n$$

where $\epsilon_i \sim \mathcal{N}(0, \sigma^2)$ are independent errors and $f(\cdot)$ is the realization a zero-mean continuous-time Gaussian Process (GP) with autocovariance $\kappa(\bar{\mathbf{x}}_i, \bar{\mathbf{x}}_j)$ [14, 11]. The estimation of a new target value y^* relies on the following property of normally distributed random vectors.

Lemma 1 (Distribution of jointly Gaussian variables). *Let z^* and \mathbf{z} be jointly Gaussian random variables:*

$$\begin{bmatrix} z^* \\ \mathbf{z} \end{bmatrix} \sim \mathcal{N}\left(\begin{bmatrix} 0 \\ \mathbf{0} \end{bmatrix}, \begin{bmatrix} \Sigma_{z^*z^*} + \sigma^2 & \Sigma_{z^*z} \\ \Sigma_{zz^*} & \Sigma_{zz} + \sigma^2 \mathbf{I}_n \end{bmatrix}\right)$$

Then, the posterior distribution of z^ conditional on z is:*

$$z^*|\mathbf{z} \sim \mathcal{N}\left(\Sigma_{z^*z} (\Sigma_{zz} + \sigma^2 \mathbf{I}_n)^{-1} \mathbf{z}, \Sigma_{z^*z^*} + \sigma^2 - \Sigma_{z^*z} (\Sigma_{zz} + \sigma^2 \mathbf{I}_n)^{-1} \Sigma_{zz^*}\right)$$

In view of the previous lemma, it is natural to use the posterior expectation as prediction rule.

$$\begin{aligned}\hat{f}(\mathbf{x}^*) &= \mathbb{E}[y^*|\mathbf{x}^*, \mathbf{y}, \mathbf{x}] = \sum_{i=1}^n c_i \kappa(\mathbf{x}^*, \bar{\mathbf{x}}_i) \\ \mathbf{c} &= (\Sigma(\mathbf{x}) + \sigma^2 \mathbf{I}_n)^{-1} \mathbf{y}\end{aligned}$$

The main distinctive feature of GP models is the learning process, which aims directly at obtaining the predictive function rather than inferring its parameters.

A zero-mean GP is completely defined by its covariance function $\kappa(\mathbf{x}_i, \mathbf{x}_j)$, also called kernel. When it is a function of the distance $r = \|\mathbf{x}_i - \mathbf{x}_j\|$ between x_i and x_j , i.e. $\kappa(\mathbf{x}_i, \mathbf{x}_j) = \kappa(r)$, the kernel is said to be stationary and isotropic. Within this class, a popular and flexible choice is the family of Matérn kernels, defined by:

$$\kappa_{\text{Matérn}}(r) = \frac{2^{1-\nu}}{\Gamma(\nu)} \left(\frac{\sqrt{2\nu}r}{l}\right)^\nu K_\nu\left(\frac{\sqrt{2\nu}r}{l}\right)$$

where ν and l are hyperparameters to be tuned and K_ν is a modified Bessel function [2]. The parameter l defines the characteristic length-scale of the process, whereas ν defines the specific covariance function in the Matérn class. If ν tends towards infinity, the Matérn formula reduces to the widely used squared exponential function

$$\kappa_{\text{se}}(r) = \exp\left(-\frac{r^2}{2l^2}\right)$$

while if $\nu = 1/2$ it becomes an exponential function

$$\kappa_{\text{exp}}(r) = \exp\left(-\frac{r}{l}\right)$$

Different approaches are possible in order to tune the hyperparameters ν , λ , and σ^2 . According to an empirical Bayes, the hyperparameter vector $\boldsymbol{\eta}$ is chosen as the maximizer of the marginal likelihood $p(\mathbf{y}|\mathbf{x}, \boldsymbol{\eta})$.

4.3 K-Nearest neighbours

K-Nearest neighbours (KNN), possibly the simplest non-linear model, relies on the distance between samples in the feature space: given a test sample \mathbf{x}_* , the prediction of y_* is computed by averaging N training samples $y_i, i \in \mathcal{C}$, where \mathcal{C} denotes the set identified by the N feature vectors \mathbf{x}_i that are closest to \mathbf{x}_* , according to some distance measure, e.g the Euclidean norm that was adopted herein.

In order to specify a KNN estimator, one has to choose the distance metric, e.g. Euclidean, Minkowsky, Manhattan, etc, and the type of weighted average, e.g. uniform or inverse distance, and to calibrate one hyperparameter, viz the number N of neighbours. Too small values of K lead to overfitting to the training data, while including too many neighbours reduces the variance at the cost of jeopardizing model flexibility.

4.4 Neural Networks

Artificial Neural Networks (ANN) are complex non-linear models, able to capture non-linear patterns and relationships. A comprehensive explanation of their structure and the most common training algorithms can be found in [7].

In this study, we focused on the Multi-Layer Perceptron (MLP) or fully connected ANN.

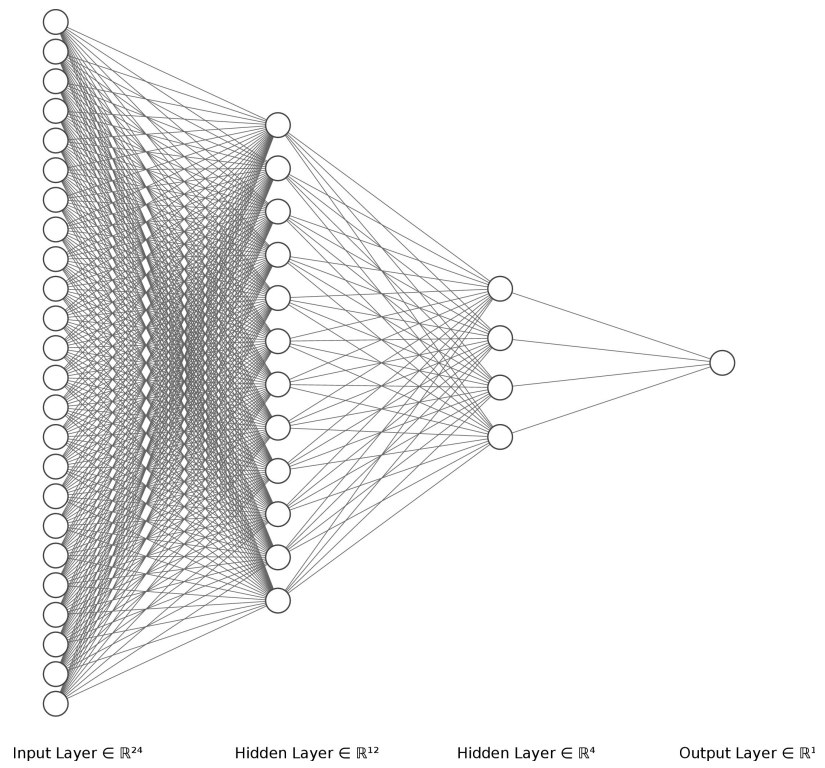


Figure 8: The ANN with 22 input features, three dense layers of 24, 12 and 4 neurons and an output neuron

The ReLu activation function and the Mean Squared Error (MSE) loss function were adopted. Training was performed by means of gradient descent as implemented in the Adaptive Moment Estimation (ADAM) algorithm [10]. The hyperparameters to be tuned include the number of neurons in each layer, the parameters entering the definition of the activation functions, and optimization parameters such as number of

epochs, batch size, and learning rate.

4.5 Torus model

The torus model [8] is a linear model based on sinusoidal functions, originally developed to predict power load. Herein, its short-term version is adapted to forecast RGD.

Following [8], a logarithmic transformation of the RGD is performed in order to mitigate the effect of its skewness. The long-term model is

$$\ln RGD^{long}(t) = L(t) + F(t) + \sum_i H_i(t)$$

where the forecast is given by the sum of three elements: the trend or level L , the potential F , which accounts for seasonality, and the effect of holidays $\sum_i H_i$.

The potential F is modelled by a linear combination of sinusoidal functions:

$$F(t) = \sum_{i=1}^{(1+2N_d)(1+2N_w)} \theta_i h_i(t), \quad \{h_i(t)\} = \mathcal{D} \otimes \mathcal{W}$$

where the functions h_i are given by the product of the j -th element in \mathcal{D} with the k -th element in \mathcal{W} , for suitable j and k , and

$$\begin{aligned} \mathcal{D} &= \{\cos(j\Psi t), j \in [0, N_d]\} \cup \{\sin(j\Psi t), j \in [1, N_d]\} \\ \mathcal{W} &= \{\cos(k\Omega t), k \in [0, N_w]\} \cup \{\sin(k\Omega t), k \in [1, N_w]\} \end{aligned}$$

The frequencies of the sinusoidal functions are $\Psi = \frac{2\pi}{365.25}$ and $\Omega = \frac{2\pi}{7}$. The number of harmonics, respectively N_w for 7-day and N_d for 365.25-day periodicity, are hyperparameters of the model.

We add to the original model the dependency on temperature, expressed in $\text{HDD}(t)$, and its daily difference $\text{HDD}(t) - \text{HDD}(t-1)$, by including these two features in the set of regressors. The terms related to trend and holidays are kept exactly as in the original work [8].

Finally, to get a short-term predictor, we correct the long-term model with the consumption of the previous day :

$$RGD(t) = RGD^{long}(t) \frac{RGD(t-1)}{RGD^{long}(t-1)}.$$

The number of harmonics N_w and N_d were tuned by minimizing the AIC index.

4.6 Technical notes on model implementation

All the models, except the torus one, were implemented in Python, using scikit-learn and keras; automated hyperparameters tuning exploited the GridSearchCV function of scikit-learn. The torus model was implemented in MATLAB, as well as its hyperparameter tuning routine.

5 Performance limit

As shown in Section 3, temperature is the most important exogenous variable. Unfortunately, the correct temperature is not available when forecasting future RGD : only a forecast is available, affected by a small yet non-negligible error, which inevitably impacts the performance of the model. The scope of this section is to assess the impact of the temperature error on the precision of RGD forecast.

Let us assume that RGD is a deterministic function g of the temperature T and some other factors $\mathbf{x} = (x_1, x_2, \dots)$: $RGD = g(T, \mathbf{x})$. In view of the analysis and the charts presented in Section 3, a reasonable first-level approximation of the relationship between RGD and T is a linear function of HDD , while the dependence on the other factors can be represented as an additive term $\bar{g}(\mathbf{x})$:

$$RGD = g(T, \mathbf{x}) = \bar{g}(\mathbf{x}) + \alpha HDD$$

where α is the sensitivity of the gas demand to the temperature expressed as HDD . The formula is of general validity and applies to both regional or national gas markets. Note that α depends on the size of the considered market and can be estimated from historical data. Consider now the ideal case when α and also the function \bar{g} are perfectly known, yet, only a forecast \hat{T} of the correct temperature T is available

$$\hat{T} = T + \epsilon$$

where ϵ is a zero-mean error with variance σ_ϵ^2 . The optimal forecast $R\hat{G}D$, given \hat{T} will obviously be:

$$R\hat{G}D = \bar{g}(\mathbf{x}) + \alpha HDD(\hat{T})$$

In order to obtain the mean square error of $R\hat{G}D$, we first compute the conditional variance of $R\hat{G}D$:

$$\begin{aligned} \text{Var}[R\hat{G}D \mid T \geq 18^\circ] &= \text{Var}[\bar{g}(\mathbf{x}) + \alpha \cdot 0] = 0 \\ \text{Var}[R\hat{G}D \mid T < 18^\circ] &= \text{Var}[\bar{g}(\mathbf{x}) + \alpha (\hat{T} - 18^\circ)] = \alpha^2 \text{Var}[\epsilon] = \alpha^2 \sigma_\epsilon^2 \end{aligned}$$

Since $\mathbb{E}[\epsilon] = 0$, it follows that $\mathbb{E}[R\hat{G}D] = RGD$. Thus:

$$\begin{aligned} \mathbb{E}\left[\left(R\hat{G}D - RGD\right)^2\right] &= P(T < 18^\circ) \text{Var}[\hat{g} \mid T < T_c] \\ &= P(T < 18^\circ) \alpha^2 \sigma_\epsilon^2 \end{aligned}$$

This last equation provides an estimate of the mean squared error due to the forecasting error on the temperatures. Since it has been derived under an ideal setting (α and $\bar{g}(\cdot)$ perfectly known) it provides a lower limit to the precision that can be achieved by the best possible forecaster.

To find a numeric value for the bound, we first estimate $P(T < T_c)$ by computing the ratio between the number of samples where $T < T_c$ is verified and the total number of available data, then we compute α through a least square fit and finally we estimate σ_ϵ^2 as the variance of the difference between the temperature forecast and the actual values. In the 3-year period 2015-2017, $P(T < T_c)$ ranges from 54% to 67%, while σ_ϵ^2 ranges from 0.05 to 0.09, and α from 9.85 to 10.96. Therefore, the mean square error is ~ 4 MSCM², that is $RMSE \sim 2$ MSCM. Indeed, the precise values, shown in Table 2, range from 1.98 to 2.15 MSCM.

6 Results

As mentioned in Section 2, available data range from 2007 to 2017. Four test sets were defined, each exactly one year long, namely 2014, 2015, 2016, and 2017. To each of them, a training set was associated, spanning from 2007 to the day before the start of the test set. Thus, training sets cover the years 2007-2013, 2007-2014, 2007-2015, 2007-2016. In the following, each training set will be identified by the year of the corresponding test set, e.g. we will write "training set 2016" to indicate the third training set, spanning from 2007 to 2015.

On each test set, the performance of each of the five models is measured using the Mean Absolute Error (MAE).

$$MAE = \frac{1}{N} \sum_{j=1}^N |RGD_j - R\hat{G}D_j|$$

MAE is preferred over MAPE due to the highly non-stationary behaviour of the series. Moreover, MAE is proportional to the monetary loss sustained by energy companies because of errors in nomination due to inaccurate forecasts.

As the performance limit derived in Section 5 poses a lower bound to the mean squared error, the Root Mean Square Error (RMSE) is also used as a comparison metric.

6.1 Hyperparameters

All the five models we considered include hyperparameters that were tuned by cross-validation.

For ridge regression, the regularization parameter λ was tuned on an interval ranging from 10^{-4} to 50 in logarithmic steps. Line search selected 0.028, 0.236, 10^{-4} and 10^{-4} as optimal values, all corresponding to 21 effective degrees of freedom [9]. Being 22 the number of features, this suggest that regularization is not relevant for our task.

For KNN we optimized the number of neighbours, in a set from 1 to 30, and the weighting strategy, choosing between uniform and inverse of distance. We obtained 9 neighbours for training set 2014, 7 for 2015 and 6 for the two remaining ones. In each set, the "inverse of distance" weights were selected.

The maximization of marginal likelihood for the GP model selected $\nu = 3/2$, $l = 10$ and $\sigma^2 = 10$, with minimal variations among all training sets.

For ANN, a grid search with 5-fold cross-validation was used not to calibrate the hyperparameters and to select the network architecture. The result was an architecture with an input layer of 24 neurons, two hidden layers of 12 and 4 neurons, and an output layer of a single neuron, as shown in Fig. 8. Moreover, we obtained a learning rate of 0.001, a number of epochs of 1000, and a batch size of 32, being the sets of possible values $\{0.1, 0.01, 0.001\}$, $\{300, 500, 1000\}$ and $\{16, 32, 64\}$, respectively.

For what concerns the torus model, the minimization of AIC and BIC led to the choice of $N_w = 3$ and $N_d = 1$ for all the training sets.

6.2 Prediction results

We first compare the performances of the adopted methods in terms of RMSE, for which a lower bound has been derived in Section 5. As the computation of the bound

requires the actual temperatures, available to us only from 2015, Table 2 only presents results achieved by the models on test sets 2015, 2016 and 2017. Considering the three years, ANN is the best model, closely followed by GP: both achieve a quite stable RMSE, just above 4 MSCM. The Torus model is also a good performer, except for the year 2015, where its error gets higher. The Ridge regression shows an higher but very stable error. Compared to a performance limit of about 2 MSCM, all the models but KNN yield an almost double RMSE. KNN achieves the poorest performance, with an RMSE of about 8 MSCM. If we consider that the limit of performance assumes ideal conditions, where the only error is the one associated with temperature forecasts, the results suggest that highly precise RGD predictions have been achieved in four cases out of five.

If we abandon the performance limit and we focus on the comparison between models, we can switch to MAE and add also the test set 2014. Out of sample results are shown in Table Table 3. Overall, GP is the best performer, achieving a MAE of 2.56 MSCM, lower than the one of ANN by 0.05 MSCM. Third is the Torus model, while ridge regression has an average MAE about 0.5 MSCM greater. KNN is again the worst model, with a MAE of 5.81 MSCM.

By comparing the classification based on MAE with the one based on RMSE, we can notice slight differences, due to the different error metrics. In case of perfectly Gaussian errors, the ratio between MAE and RMSE is known to be $\sqrt{2/\pi} \sim 0.8$. However, if we compute such a ratio for each model, we get lower results: about 0.61 for GP and Torus, 0.65 for KNN and ANN and 0.71 for Ridge. This is explained by the "fat tails" of the error distributions, highlighted in Fig. 9.

Due to the seasonal behaviour of RDG, it may be of interest to study the monthly errors. In Table 4 we show the average of the absolute errors achieved by each model in each month, throughout the four test sets. It is clear that GP is the best performer during the summer period, especially from May to September, whereas in the other months ANN is more accurate. This leads us to the conclusion that the GP model is better at capturing the effects of the weekly seasonality, while ANN can better take into account the non-linear effect of temperature, mostly relevant during the cold months.

As mentioned before, to the best of our knowledge, there are no benchmarks in the literature for the task we performed. However, Zhu et al. [21] performed short-term forecasting of UK demand. Performances are still not completely comparable, for two main reasons: first, the authors considered the whole UK demand, and not only the residential demand; second, UK climate is colder and less variable than the Italian one. Nonetheless, we can use a relative error metrics, such as Mean Absolute Percentage Error (MAPE), to try and compare model performances only on 6 cold months (from October to March). Our best model in terms of MAPE, the ANN, achieves a 3.15% MAPE, while Zhu's false neighbours filtered-support vector regression local predictor (FNF-SVRLP) reaches a 3.88 % MAPE on the 6 months.

Model	year 2015	year 2016	year 2017
Ridge	4.67	4.39	4.31
GP	4.33	4.28	4.14
KNN	7.82	8.05	8.72
Torus	5.31	4.32	3.93
ANN	4.34	4.11	3.64
Physical limit	2.15	2.02	1.98

Table 2: Yearly Root Mean Squared Error (RMSE) on test sets and performance limit

Model	year 2014	year 2015	year 2016	year 2017	Average
Ridge	3.20	3.34	3.15	3.00	3.17
GP	2.46	2.65	2.58	2.56	2.56
KNN	6.94	5.39	5.42	5.48	5.81
Torus	2.38	3.18	2.66	2.54	2.69
ANN	2.58	2.76	2.68	2.43	2.61

Table 3: Yearly Mean Absolute Error (MAE) on test sets

Month	Ridge	GP	KNN	Thorus	ANN
January	5.48	5.24	11.31	5.85	5.06
February	4.71	4.66	9.37	5.31	4.5
March	4.7	5.09	9.55	4.32	5.1
April	3.61	3.13	8.85	2.95	3.13
May	2.5	1.24	2.96	1.49	1.25
June	1.46	0.5	2.24	1.04	0.67
July	1.14	0.35	1.18	0.46	0.51
August	2.23	0.7	5.05	0.93	1.08
September	1.9	0.36	1.25	0.47	0.74
October	2.27	1.63	3.91	1.87	1.89
November	3.26	3.56	6.83	3.34	3.18
December	4.87	4.39	7.41	4.36	4.29

Table 4: Monthly Mean Absolute Error (MAE) on test sets: best performers are highlighted with boldface



Figure 9: Out-of-sample model residuals in 2017

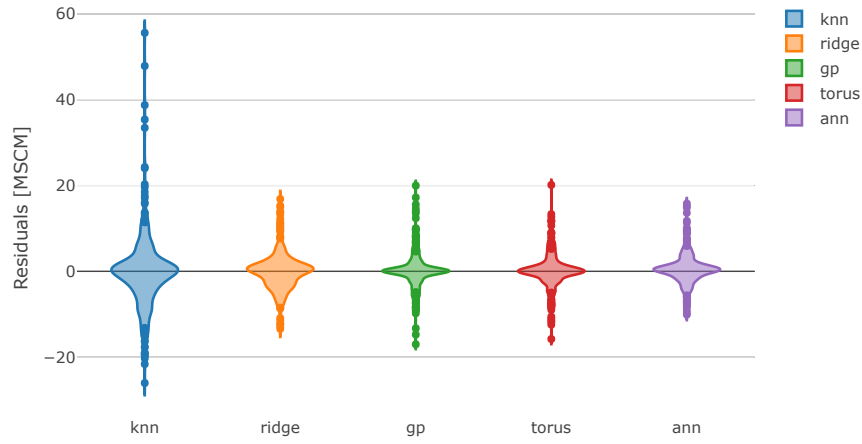


Figure 10: Distribution of out-of-sample residuals in 2017

7 Conclusion

In this paper, we faced the task of forecasting one-day-ahead the daily Italian residential gas demand. We presented the main features of the time series and its covariates, such as temperature, and the most relevant steps of preprocessing and feature extraction. Then, we described and compared five different statistical learning models:

Ridge regression, Gaussian Processes, K-nearest neighbour, Artificial Neural Networks and a Toroidal model.

As no benchmark was available for the specific task, we derived a theoretical performance limit, based on the inaccuracy of meteorological forecasts, which was then used as the ultimate benchmark for the models. Our best model, in terms of RMSE, the deep neural network, achieves an error which is about double with respect to the performance limit. On the other hand, looking at the MAE such as error measure, the GP is the best model. From the analysis of monthly performance, we realize that GP model is more accurate in following the weekly seasonality, the predominant effect in the summer period, while the deep neural network can better take into account the non-linear influence of temperature, whose contribution is greater during the winter period.

References

- [1] Italian natural gas demand report. <http://pianodecennale.snamretegas.it/it/domanda-offerta-di-gas-in-italia/domanda-di-gas-naturale.html>. Accessed: 2019-01-31.
- [2] Milton Abramowitz and Irene A Stegun. *Handbook of mathematical functions: with formulas, graphs, and mathematical tables*, volume 55. Courier Corporation, 1965.
- [3] A Azadeh, SM Asadzadeh, and A Ghanbari. An adaptive network-based fuzzy inference system for short-term natural gas demand estimation: uncertain and complex environments. *Energy Policy*, 38(3):1529–1536, 2010.
- [4] Marek Brabec, Ondřej Konár, Emil Pelikán, and Marek Malý. A nonlinear mixed effects model for the prediction of natural gas consumption by individual customers. *International Journal of Forecasting*, 24(4):659–678, 2008.
- [5] Ömer Fahrettin Demirel, Selim Zaim, Ahmet Çalışkan, and Pınar Özuyar. Forecasting natural gas consumption in istanbul using neural networks and multivariate time series methods. *Turkish Journal of Electrical Engineering & Computer Sciences*, 20(5):695–711, 2012.
- [6] Salvador Gil and J Deferrari. Generalized model of prediction of natural gas consumption. *Journal of energy resources technology*, 126(2):90–98, 2004.
- [7] Ian Goodfellow, Yoshua Bengio, and Aaron Courville. *Deep Learning*. MIT Press, 2016. <http://www.deeplearningbook.org>.
- [8] Alice Guerini. Long and short term forecasting of daily and quarter-hourly electrical load and price data: a torus-based approach. page xxx, 2016.
- [9] T. Hastie, R. Tibshirani, and J. Friedman. *The Elements of Statistical Learning: Data Mining, Inference, and Prediction, Second Edition*. Springer Series in Statistics. Springer New York, 2009.
- [10] Diederik P Kingma and Jimmy Ba. Adam: A method for stochastic optimization. *arXiv preprint arXiv:1412.6980*, 2014.
- [11] K.P. Murphy and F. Bach. *Machine Learning: A Probabilistic Perspective*. Adaptive Computation and Machi. MIT Press, 2012.
- [12] Ioannis P Panapakidis and Athanasios S Dagoumas. Day-ahead natural gas demand forecasting based on the combination of wavelet transform and anfis/genetic algorithm/neural network model. *Energy*, 118:231–245, 2017.
- [13] Primož Potočnik, Marko Thaler, Edvard Govekar, Igor Grabec, and Alojz Poredoš. Forecasting risks of natural gas consumption in slovenia. *Energy policy*, 35(8):4271–4282, 2007.

- [14] C.E. Rasmussen and C.K.I. Williams. *Gaussian Processes for Machine Learning*. Adaptative computation and machine learning series. University Press Group Limited, 2006.
- [15] Dario Šebalj, Josip Mesarić, and Davor Dujak. Predicting natural gas consumption—a literature review. In *28th International Conference "Central European Conference on Information and Intelligent Systems"*, 2017.
- [16] Božidar Soldo. Forecasting natural gas consumption. *Applied Energy*, 92:26–37, 2012.
- [17] Božidar Soldo, Primož Potočnik, Goran Šimunović, Tomislav Šarić, and Edvard Govekar. Improving the residential natural gas consumption forecasting models by using solar radiation. *Energy and buildings*, 69:498–506, 2014.
- [18] Jolanta Szoplik. Forecasting of natural gas consumption with artificial neural networks. *Energy*, 85:208–220, 2015.
- [19] Fatih Taşpinar, Numan Celebi, and Nedim Tutkun. Forecasting of daily natural gas consumption on regional basis in turkey using various computational methods. *Energy and Buildings*, 56:23–31, 2013.
- [20] Zlatko Tonković, Marijana Zekić-Sušac, and Marija Somolanji. Predicting natural gas consumption by neural networks. *Tehnički vjesnik*, 16(3):51–61, 2009.
- [21] Lixing Zhu, MS Li, QH Wu, and L Jiang. Short-term natural gas demand prediction based on support vector regression with false neighbours filtered. *Energy*, 80:428–436, 2015.